ARTICLE

New members of metallocene radical bridged dilanthanide single-molecule magnets based on the unsubstituted 1,2,4,5-tetrazine ligand

Received 00th January 20xx,
Accepted 00th January 20xx

DOI: 10.1039/x0xx00000x

Niki Mavragani, [a] Alexandros A. Kitos, [a] Akseli Mansikkamäki[b] and Muralee Murugesu* [a]

Through a stepwise synthetic procedure, the combination of the unsubsituted 1,2,4,5-tetrazine (tz) with lanthanide metallocenes yielded a new family of radical-bridged dinuclear complexes; $[(Cp^*_2Ln^{III})_2(tz^{\bullet-})(THF)_2](BPh_4)$, (Ln = Gd (**1**), Tb (**2**), Dy (**3**); THF = tetrahydrofuran; Cp* = pentamethylcyclopentadienyl). The strong magnetic exchancge coupling of $J_{Gd\text{-}rad}$ = -7.2 cm^{-1} observed in **1**, was probed through SQUID magnetometry as well as computational studies. This in combination with the highly anisotropic oblate Tb^{III} and Dy^{III} ions in **2** and **3**, respectively, lead to zero-field SMM behaviour and slow relaxation of the magnetization through thermally activated processes.

Introduction

For more than thirty years, single-molecule magnets (SMMs) have proven to be prosperous candidates as switchable, molecular devices for storage information by using the orientation of their spins.[1–3] Although the field of Molecular Magnetism started from the study of 3*d*-based systems,[4] it flourished upon switching towards 4*f*-based systems. Bistability of their magnetic ground state in addition to large inherent anisotropy has set 4*f* ions as protagonists in the field of Molecular Magnetism.[5,6] Lanthanide-based SMMs have been known to yield longer relaxation times of their magnetization and large thermal barriers to spin reversal (U_{eff}), subsequently leading to magnetic remanence at higher temperatures.[7–9] Over the past decade, the targeted design of Ln systems for achieving superior SMM behaviour, such as increasing the axiality of the ligand field (LF) around the metal centres, has enabled important scientific breakthroughs.[10] In particular, it is well established that increasing the axiality of the ligand field in oblate Tb^{III} and Dy^{III} ions can lead to larger thermal barriers.[11] While these features could lead to spin-based information storage, research has mostly focused on mononuclear SMMs.[9,12] Consequently, the switch towards the synthesis of polynuclear Ln-complexes with optimum magnetic properties presupposes the use of multidentate bridging ligands.

In addition to this, the design of next generation SMMs, premises that through barrier relaxation of the magnetization needs to be minimized (such as quantum tunnelling of the magnetization -QTM-, Raman and direct mechanisms).[3] This can be surpassed by the presence of strong magnetic communication between the Ln centres. The importance of the magnetic communication in the form of a meta-metal bond was recently reported by Gould *et al.* in $(Cp^{iPr5})_2Ln_2I_3$ (Ln = Gd, Tb, Dy; Cp^{iPr5} = pentaisopropylcyclopentadienyl), which exhibited an enormous coercive field (> 14 T) at temperatures as high as 60 K.[13] However, controlling the formation of metal-metal bonds is rather unrealistic. A promising alternative to this relies on the exploitation of open shell ligands, which benefits from the magnetic Ln-rad coupling. Given that the latent is strong enough the successful suppression of through-barrier relaxation of the magnetization can be achieved. Indeed, this approach has led to increased magnetic performance as strong Ln-radical coupling has been shown to lead to higher blocking temperatures of the magnetization (up to 20 K) and significant magnetic hardness (H_c = 7.9 T).[14] Strong exchange coupling between the diffuse spin of the radicals and the lanthanide centres gives rise to a high angular momentum ground state of the single magnetic unit by minimizing single-ion effects (i.e. QTM). To this day, several attempts towards this direction have been made,[15–18] with the $N_2^{\bullet 3-}$ radical bridged family having the best magnetic performance, yet reported.[14,19] However, the isolation of $N_2^{\bullet 3-}$ radical bridged complexes is a synthetic challenge as it cannot, rationally, be incorporated into complexes, and it offers no room for structural modification.

Recently, we demonstrated that the incorporation of the 1,2,4,5-tetrazine (tz) into tetranuclear **"Ln_4"** metallocenes ($[(Cp^*_2Ln)_4(tz^{\bullet-})_4]\cdot 3(C_6H_6)$, where Ln = Dy and Gd; Cp* = pentamethylcyclopentadienyl), can lead to strong magnetic coupling and significant magnetic hardness (H_c = 3 T).[20] Apart from the synthetic advances over the $N_2^{\bullet 3-}$ radical bridge, the very low-lying π^* LUMO of the tz ring, can easily undergo a one e^- reduction, forming the $tz^{\bullet-}$ radical anion.[21] The diffuse nature of the spin orbitals of $tz^{\bullet-}$-based radicals are ideally suited to penetrate the shielded 4*f* orbitals, promoting strong coupling.[22]

[a] Department of Chemistry and Biomolecular Sciences, University of Ottawa, Ottawa, ON K1N 6N5, Canada. E-mail: m.murugesu@uottawa.ca.
[b] NMR Research Unit, University of Oulu, P.O. Box 300, 90014 Oulu, Finland.

Electronic Supplementary Information (ESI) available: Synthetic procedures, single-crystal X-ray diffraction data, additional magnetic and computational data. CCDC numbers 2202463-2202465. For ESI and crystallographic data in CIF or other electronic format see DOI: 10.1039/x0xx00000x.

However, a strongly coupled polynuclear Ln_4 system is complicated enough to examine the effect of the Ln-radical coupling and therefore, lowering the nuclearity might shed more light into the direct correlation of magnetic exchange interactions and the magnitude of the thermal barrier to magnetic relaxation.

With these in mind, our efforts involve the use of the $tz^{\bullet-}$ as a bridging ligand to connect $[Cp^*_2Ln^{III}]^+$ moieties, which are characterized by significant magnetic axiality. Herein, we report the employment of the unsubstituted $tz^{\bullet-}$ for the first time in dinuclear lanthanide metallocene complexes, yielding: $[(Cp^*_2Ln^{III})_2(tz^{\bullet-})(THF)_2](BPh_4)$, (Ln = Gd (**1**), Tb (**2**), Dy (**3**); THF = tetrahydrofuran). Strong antiferromagnetic coupling between the $tz^{\bullet-}$ and the Ln^{III} centres is observed for all three complexes, yielding zero-field SMM behaviour with slow relaxation of the magnetization and magnetic hysteresis for **2** and **3**. Based on *ab initio* calculations the strong antiferromagnetic Ln-rad coupling is probed, verifying that their magnetic state can be interpretated as a giant-spin where the relaxation of the magnetization is related to changes in the magnetic state of the overall exchange-coupled system.

Results and discussion

Synthetic procedure and structural description

The first step, in the synthesis of **1**-**3**, involves the equimolar reduction of the tz ligand with potassium graphite (KC_8) in THF (Scheme 1). The dark mixture is slowly added to a solution of two equivalents of $[Cp^*_2Ln^{III}][(\mu\text{-}Ph_2)BPh_2]$ (where Ln = Gd (**1**), Tb (**2**), Dy (**3**)). The resulting dark red solution was stirred overnight, filtered and placed in an Et_2O bath. After two days, dark red crystals of $[(Cp^*_2Ln^{III})_2(tz^{\bullet-})(THF)_2](BPh_4)$, (Ln = Gd (**1**), Tb (**2**), Dy (**3**)) were obtained (Fig. S1).

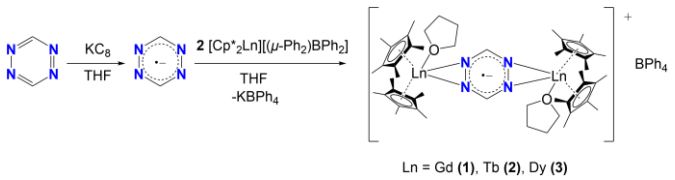

Scheme 1 Synthesis of the radical-bridged dinuclear compounds (**1**-**3**).

Single-crystal X-ray diffraction (SCXRD) analysis reveals that **1**-**3** crystallize in the monoclinic *I*2/a space group as centrosymmetric dinuclear complexes, with one crystallographically independent Ln^{III} center. Selected bond distances and angles along with X-ray data of all complexes are summarized in Tables S1-S2. The three cationic complexes are isomorphous (Fig. S2) and therefore, only **3** is presented in Fig. 1. The complexes consist of two $[Cp^*_2Ln^{III}]^+$ moieties, bridged by a μ-$tz^{\bullet-}$ ligand. The coordination sphere of each Ln^{III} centre is completed by one THF molecule (av. $Ln–O_{THF}$: 2.389(2) Å). To stabilize the cationic complex, one BPh_4^- is found in the crystal lattice. The average $Ln–C_{Cp^*}$ bond distances are 2.707(1), 2.687(2) and 2.678(1) Å for complexes **1**-**3**, respectively, while the $Cp^*_{cent}–Ln–Cp^*_{cent}$ angles are 136.3(2)°, 136.4(2)° and 136.6(2)°. These bond distances and angles highlight the fact

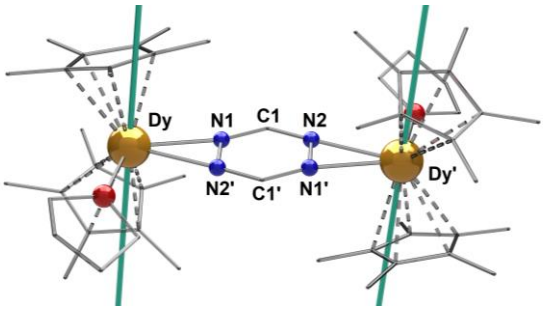

Fig. 1 Molecular structure of **3**. Partial labelling and omission of the BPh_4^- moiety and H-atoms have been employed for clarity. The solid teal lines represent the orientation of the principal magnetic axes of the ground Kramers doublet. Colour code: C: light grey; N: blue; O: red; Dy: orange.

that the axiality imposed by the Cp^* ligands is increasing along the lanthanide series. These values are similar to those reported for other radical bridged SMMs containing $[Cp^*_2Ln]^+$ moieties, which usually display high single-ion anisotropy.[18,23,24] The average $Ln–Cp^*_{cent}$ distances (2.427(5), 2.405(5) and 2.395(5) Å for **1**-**3**, respectively) and $Ln–N_{tz}$ bond distances (2.485(3), 2.469(2) and 2.460(2) Å for **1**-**3**, respectively) are close to the respective distances for the reported **"Ln_4"** complexes (av. $Ln–Cp^*_{cent}$: 2.403(1) Å and av. $Ln–N_{tz}$: 2.601(4) Å).[20] These $Ln–N_{tz}$ bond distances are also similar to those observed for bipyrimidyl radical-bridged complexes (2.424(6) – 2.440(6) Å)[18,25], but, as expected, they are larger upon comparison to the $N_2^{\bullet3-}$ systems (2.234(1) Å).[14,19] The reduction of the tz ligand is confirmed through charge balance considerations, as well as the elongation of the N–N bonds of the tetrazine ring which is significant when compared to the free ligand.[26] The average N1–N2' bond distance in **1**-**3** range from 1.391(3) to 1.394(3) Å. Such N–N bond elongations have been previously reported for $tz^{\bullet-}$-based ligands.[20,27]

Inspection of the packing arrangement of all three compounds reveals that these dimers are in relatively close proximity (Fig. S3). A thorough study of the supramolecular organization of the Ln_2 units *via* Hirshfeld surface analysis[28] is given in the ESI (Fig. S3, S4). The absence of strong hydrogen bonding donors or acceptors in both the main residue and solvent area of **1**, **2** and **3** leads mostly to close packing interactions such as C···H/H···C and H···H interactions with total percentages of 12% and 88%, respectively, as revealed by the 2D fingerprint plots of all interatomic interactions (Fig. S4). Notably, the average shortest intermolecular Ln···Ln distance is 9.505(6) Å, while the respective average intramolecular distance is 7.099(5) Å (Fig. S5).

Magnetic properties

To probe the magnetic behaviour of **1**-**3**, direct current (dc) and alternating current (ac) magnetic susceptibility studies were undertaken. The dc magnetic susceptibilities of all complexes were measured between 300 and 1.8 K at 1000 Oe (Fig. 2). At room temperature, the χT products are 16.11 cm^3 K mol^{-1}, 23.96 cm^3 K mol^{-1} and 28.58 cm^3 K mol^{-1} for **1**-**3**, respectively. These are consistent with the theoretical values of 16.13 cm^3 K mol^{-1}, 24.01 cm^3 K mol^{-1} and 28.71 cm^3 K mol^{-1} for **1**-**3**, respectively, for

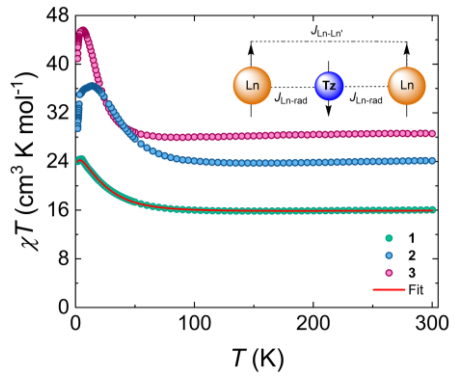

Fig. 2 Variable temperature dc susceptibility of **1** (teal circles), **2** (blue circles) and **3** (magenta circles) under an applied field of 1000 Oe. The solid red line represents the fit as determined from the application of the 2*J* formalism. Insert: Simplified illustration of the two *J*-model which was used to fit the data highlighting the antiparallel spin alignment of the Ln^{III} ions with respect to the $tz^{\bullet-}$ ligand. Colour code: Ln^{III}: orange spheres; $tz^{\bullet-}$: blue spheres.

two Ln^{III} ions (Gd: $S = 7/2$, $^8S_{7/2}$, $g = 2$, $C = 7.88$ cm³ K mol⁻¹ ; Tb: $S = 3$, $L = 3$, $^7F_6$, $g = 3/2$, $C = 11.82$ cm³ K mol⁻¹; Dy: $S = 5/2$, $L = 5$, $^6H_{15/2}$, $g = 4/3$, $C = 14.17$ cm³ K mol⁻¹) and one radical moiety ($S = ½$, $C = 0.37$ cm³ K mol⁻¹). Upon lowering of the temperature, the χT product slightly decreases until ~145 K for **1**, ~150 K for **2** and ~90 K for **3** reaching a shallow minimum (15.85 cm³ K mol⁻¹, 23.4 cm³ K mol⁻¹ and 27.97 cm³ K mol⁻¹, for **1**-**3** respectively). Above that temperature, it starts to increase rapidly upon further lowering of the temperature, until it reaches a maximum of 24.43 cm³ K mol⁻¹ at 5 K for **1,** 35.83 cm³ K mol⁻¹ at 14 K for **2** and 45.6 cm³ K mol⁻¹ at 6.5 K for **3**. This behaviour can be attributed to the spin alignment of the Ln ions which is caused by the strong antiferromagnetic interactions between the metal centres and the $tz^{\bullet-}$ ligand (Fig. 2, insert).[20,23,25] Bellow this temperature, the χT value decreases slowly for **1** and rapidly for **2** and **3** with the temperature drop until it reaches a value of 24.02 cm³ K mol⁻¹, 29.15 cm³ K mol⁻¹ and 40.93 cm³ K mol⁻¹ at 1.8 K, respectively. For **2** and **3**, this steep downturn in the lower temperature region is attributed to magnetic blocking as observed for similar lanthanide systems.[25]

To validate the presence of magnetic blocking, zero-field-cooled/field-cooled (ZFC/FC) magnetic susceptibility measurements were performed for **2** and **3**. For both complexes, the divergence of the two data sets, at 3.4 K for **2** and 2.2 K for **3**, confirms the pinning of the magnetic moment below these temperature regions (Fig. S7). Field dependence of the magnetization (up to 70 kOe) at different temperatures (1.9 to 7 K) was measured for all three complexes. For **2** and **3**, distinct *s*-shape curves were observed in the isotemperature lines at 1.9 and 3 K for **2** and 1.9 K for **3** (Fig. S8), clearly suggesting the presence of magnetic blocking. Consequently, magnetic hysteresis measurements were performed for **2** and **3** to confirm the observed trends for both complexes. Using an average sweep rate of 25 Oe/s, the magnetic hysteresis was measured between 70 to -70 kOe in the temperature range of 1.8 to 3.8 K for **2** and 1.8 to 3.5 K for **3** (Fig. S9). For both complexes at 1.8 K and zero field, the butterfly-shaped hysteresis loops are waste restrained. This type of crossing at $H_{dc} = 0$ Oe is often attributed to QTM which is also expected to be present in the ac magnetic susceptibility of **2** but not for **3** (non-Kramers *vs.* Kramers ion). Upon increase of the field, the opening of the loops is observed. The loops remain open until 3.8 K for **2** and 3.5 K for **3**, above which they are no longer open.

As already mentioned, blocking of the magnetization can result from a high-angular momentum ground state arising from the strong antiferromagnetic coupling between the radical bridging ligand and the lanthanide ions. The isotropic nature of the $4f^7$ electron configuration of the Gd^{III} centres in **1** allows for the quantification of the magnetic exchange coupling. The dc magnetic susceptibility data of **1** were fitted with the PHI software,[29] to the spin-only Hamiltonian: $\hat{H} = -2J_{Gd\text{-}rad}\hat{S}_{rad}(\hat{S}_{Gd} + \hat{S}_{Gd'}) - 2J_{Gd\text{-}Gd'}\hat{S}_{Gd}\hat{S}_{Gd'}$, where $J_{Gd\text{-}rad}$ represents the Gd^{III}-radical exchange coupling, $J_{Gd\text{-}Gd'}$ represents the intramolecular Gd^{III}-Gd^{III} exchange coupling and $\hat{S}_i$ are the spin operators for each paramagnetic centre. The best fit afforded $J_{Gd\text{-}rad} = -7.2$ cm⁻¹, confirming the anticipated antiferromagnetic Gd^{III}-radical coupling. Additionally, due to the strong antiferromagnetic alignment of the Ln spins with the radical, the best fit yielded $J_{Gd\text{-}Gd} = 0.32$ cm⁻¹, indicating ferromagnetic coupling between the Ln^{III} centres. This is further validated by the field-dependent magnetization measurements for **1** at low temperatures. The magnetization plot (*M vs. H*, Fig. S8) shows field dependence, as it increases rapidly upon increasing the field, reaching a value of 13.84 $N\mu_B$ at 1.9 K and 7 T, which supports a spin ground state of $S_T = 13/2$. Surprisingly, this value is comparable to even some dinitrogen-bridged complexes with similar exchange strengths (-7.2 and -7.3 cm⁻¹).[14] Since similar trends were observed in the temperature dependence of the χT data for **2** and **3** (*vide supra)* it can be assumed that they also exhibit strong antiferromagnetic Ln^{III}-$tz^{\bullet-}$ coupling (*vide infra*).

Due to the strong antiferromagnetic Ln-radical coupling, ac magnetic susceptibility measurements for **2** and **3** were undertaken to investigate their SMM behaviour. For both complexes, a temperature-dependent ac susceptibility signal was observed in the absence of a magnetic field ($H_{dc} = 0$ Oe) in the frequency range of 0.1 to 1500 Hz. For **2**, both the in-phase (χ') (Fig. S10) and out-of-phase (χ'') (Fig. 3A) susceptibilities show frequency-dependent behavior between 8 and ~4.2 K, which is indicative of a thermally activated mechanism. Below that temperature (4 to 1.8 K), the overlap of the χ'' signal, as well as the little frequency-dependence of the peak of the susceptibility, suggest that QTM effects are dominating the relaxation of the magnetization in that temperature region. Fitting of the ac susceptibility data for **2** (when $H_{dc} = 0$ Oe) using CCFit-2 software[30] (Fig. 3B) to a generalized Debye model, afforded the relaxation times (τ) (Table S3). Insight into the magnetic relaxation dynamics of **2** in the absence of a static dc field, was gained by the analysis and fitting of the τ *vs.* T plots (Fig. 3C). For **2**, a combination of QTM and Orbach mechanisms was used to accurately fit the relaxation times, using eq. (1):

$$\tau^{-1} = \tau_{QTM}^{-1} + \tau_0^{-1}\exp(-U_{eff}/k_BT) \quad (1)$$

where, τ is the magnetic relaxation time, τ_{QTM} is the relaxation time for quantum tunnelling, τ_0 is the attempt time and U_{eff} is the effective barrier to spin reversal. A term accounting for

ARTICLE

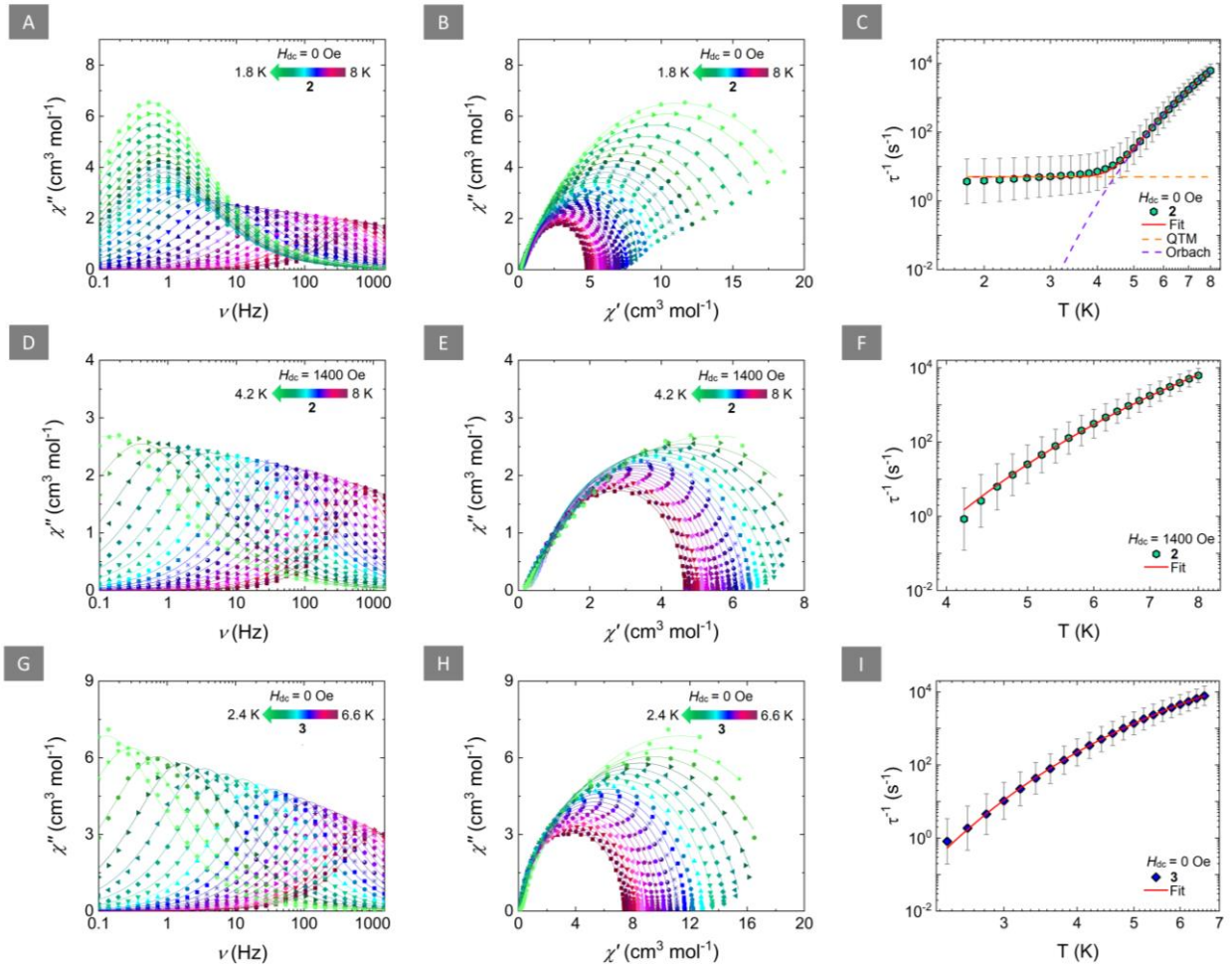

Fig. 3 Left: Frequency-dependence of the out-of-phase magnetic susceptibility (χ'') for **2** (H_{dc} = 0 Oe; (A); H_{dc} = 1400 Oe; (D)) and **3** (H_{dc} = 0 Oe; (G)) at the respective temperature regions. Solid lines represent fits to the generalized Debye model. Middle: Cole-Cole plots for **2** (H_{dc} = 0 Oe; (B); H_{dc} = 1400 Oe; (E)) and **3** (H_{dc} = 0 Oe; (H)) at the respective temperature regions. Solid lines represent fits to the generalized Debye model. Fitting parameters for the generalized Debye fit of the ac susceptibilities are summarized in Tables S3, S5 and S6, respectively. Right: Temperature-dependence of the relaxation times (τ) for **2** (H_{dc} = 0 Oe; (C); H_{dc} = 1400 Oe; (F)) and **3** (H_{dc} = 0 Oe; (I)) with the respective estimated standard deviations (gray bars). The estimated standard deviations of the τ were calculated from the α-parameters of the generalized Debye fits and the log-normal distribution as described in reference [30]. The solid red lines represent the best-fit based on eq. (1) for (C) and eq. (2) for (F) and (I), while the dashed orange and purple lines in (C) represent the individual components of the magnetic relaxation for QTM and Orbach processes, respectively.

Raman relaxation was also investigated, without improving the fit, or providing any physically meaningful parameters and was therefore removed. The best fit for **2** yielded τ_{QTM} = 0.20 s, τ_0 = 2.33 × 10^{-8} s and U_{eff} = 49.2 cm^{-1}.

To probe the effect of an applied static field in the relaxation process of **2**, ac measurements were undertaken at various static fields (0-3000 Oe). At a constant temperature of 4.5 K, a field-dependent signal of the χ'' of **2** was observed (Fig. S11). Fitting of the χ'' *via* a generalized Debye model yielded the field-dependent relaxation times of **2** (Table S4). As evident by Fig. S12, the relaxation times are increasing with the increase of the applied static field between 0 and 1400 Oe. At higher fields, the relaxation times become field independent, indicating that beyond this field, single-ion effects such as QTM have been successfully suppressed and the relaxation of the magnetization is indeed mediated *via* the thermally activated pathway.

Since the presence of a static field can lead to effective suppression of QTM in **2**, ac susceptibility measurements at 1400 Oe between 8 and 4.2 K were performed (Fig. 3D, 3E and S13). Fitting of the ac susceptibility for **2** (when H_{dc} = 1400 Oe)

via a generalized Debye model, yielded longer relaxation times (Tables S5). As expected, the peaks of the susceptibility showed an exponential increase upon lowering of the temperature, indicative of a thermally activated relaxation process, i.e. Orbach mechanism. As such, the relaxation times were fitted, using eq. (2) (Fig. 3F):

$$\tau^{-1} = \tau_0^{-1}\exp(-U_{eff}/k_BT) \quad (2)$$

The best-fit parameters were $\tau_0 = 1.35 \times 10^{-8}$ s and $U_{eff} = 51.9$ cm^{-1}. Accordingly, the Arrhenius plot of the ln(τ) *vs.* the inverse of temperature was constructed to verify these findings (Fig. S14). The linear fit of Arrhenius plot reveals a $U_{eff} = 53.3$ cm^{-1} which is in good agreement with the fits obtained using eq. (2).

Comparatively, the ac susceptibility for **3** in the absence of a static dc field (H_{dc} = 0 Oe) showed frequency-dependent in a smaller temperature region (6.6 to 2.4 K) (Fig. 3G and S15). Fitting of the ac susceptibility data for **3** (Fig. 3H) afforded the τ (Table S6) which were further analyzed and fitted using eq. (2) (Fig. 3I). The best-fit for **3**, yielded significantly smaller parameters than **2**, with $\tau_0 = 5.61 \times 10^{-7}$ s and $U_{eff} = 25.0$ cm^{-1}. The linear fit of the respective Arrhenius plot for **3** afforded an effective barrier to spin reversal of $U_{eff} = 24.8$ cm^{-1} which is in good agreement with the fits obtained using eq. (2) (Fig. S16).

Contrary to **2**, the field-dependence of the χ'' susceptibility of **3** (Fig. S17), upon fitting with a generalized Debye model (Table S7), yielded, relatively constant the relaxation times which were, as expected, altogether not affected by the variation of the applied static field (Fig. S18). The superposition of the field-dependent ac susceptibility signals and the non-improvement of the signal with the increase of the applied field further confirms the undoubtable presence of an Orbach-only mediated magnetic relaxation which is expected to be extremely weak field-dependent.

The U_{eff} that were obtained for **2** and **3** (Table S8) are higher compared to other tetrazine-based radical bridged lanthanide systems[15,16,27] but are modest in comparison to the **"Ln$_4$"** tetranuclear tz$^{\bullet}$-bridged system[20] or other radical bridged systems.[14,18,19] This is probably attributed to the presence of the coordinated THF. The Ln-O_{THF} distances (2.388(2)-2.376(2) Å) is comparable to the Ln-N_{tz} distances (2.453(2)-2.445(2) Å). These equatorial contributions are significant enough to compete with the axiality imposed by the Cp* ligands, thus lowering the overall SMM performance. As such, removing these coordinated solvents is expected to enhance the SMM properties. However, efforts to remove the coordinated THF solvent molecules were not successful as complexes were not preserved and, thus, the THF-free dimers could not be isolated.

Computational studies

To validate the observed magnetic behavior of **1**-**3**, the metal–radical exchange interaction was studied by computational methods. The isotropic exchange coupling parameters in **1** were calculated by both broken-symmetry density functional theory (BS-DFT)[31–36] using the CAM-B3LYP functional[37–39] and the Orca code.[40–42] The metal–radical and metal–metal exchange couplings were calculated as $J_{M-R} = -10.7$ cm^{-1} and $J_{M-M} = -7.5$ cm^{-1}, respectively. While the metal–radical exchange is in reasonable agreement with the value obtained from the fit (–14.4 cm^{-1}, 0.64 cm^{-1}), the metal–metal interaction is unreasonably large. The origin of this discrepancy could not be determined but based on various test calculations, it was not a functional-dependent effect. In order to get a more reliable computational estimate of the exchange interaction, the metal–radical exchange parameter was also calculated at NEVPT2//SA-CASSCF(13,13) level (see the ESI for further details).[40–48] The calculated value is $J_{M-R} = -12.3$ cm^{-1}, which is in reasonable agreement with the fitted value although slightly underestimated. It is typical that SA-CASSCF calculations underestimate the kinetic exchange contribution to the exchange interaction and therefore underestimate the strength of anti-ferromagnetic coupling. Powder-magnetic susceptibility simulated from the calculated parameter leads to a good agreement with the experimentally observed susceptibility (Figure S19).

The strong magnetic anisotropy arising from the first-order orbital contribution to the magnetic moment in **2** and **3** makes analysis of the exchange coupling considerably more difficult. The energy spectrum of the Hamiltonian of the full complex was constructed from NEVPT2//SA-CASSCF//QDPT calculations[40–50] treating one metal–radical interaction while the other metal ion was replaced by the diamagnetic Y^{III} ion. The procedure is based on mapping of the *ab initio* states to pseudospin states and on construction of a pseudospin Hamiltonian.[51] Unlike the commonly used Lines model that is valid only at the weak exchange limit,[52] the present model utilizes the full exchange tensor that is valid also for strong exchange interaction.[51] The present approach differs from earlier *ab initio* treatments of the full lanthanide–radical exchange interaction[53–55]in that it is completely based on multireference calculations and does not require any fitted or DFT-based parameters. The disadvantage of the approach is that in its present form it does not give a direct access to the different components of the exchange tensor. Details of the process are given in the ESI. The magnetic susceptibilities calculated using the pseudospin Hamiltonian are in reasonable agreement with the experimentally observed susceptibilities (Figure S19). This agreement along with the agreement between the calculated and fitted exchange coupling constants for **1** show that the model is reliable.

The energies and properties of the four lowest Kramers doublets of **2** and **3** are described in Table S11 and Table S12. The energies of the first excited KDs of both **2** and **3** (38 cm^{-1} and 21 cm^{-1}, respectively) are in reasonable agreement with the observed barrier heights (49 cm^{-1}, 26 cm^{-1}). The values are slightly underestimated due to the slight underestimation of the strength of the anti-ferromagnetic exchange as is the case in **1**. Thus, the relaxation of magnetization most likely proceeds *via* the first excited KDs. The calculated transition magnetic moment matrix elements[56] show that in the case of **2**, the barrier crossing takes place earliest at the first excited KD and latest at the second excited KD (Figure S20). In the case of **3**, the barrier could not be reliably reproduced and suggest that QTM is the main relaxation mechanism. The discrepancies in the calculated barriers most likely originate from numerical inaccuracies. Analysis of the **g** tensors shows that the ground KD

corresponds to an Ising-type ferrimagnetic spin configuration where the metal magnetic momenta are aligned in the same direction and the radical moment in the opposite direction. The first excited KD corresponds to a situation where one of the metal moments has flipped so that the metal moments lie in opposite directions. Therefore, the magnetic relaxation is related to changes in the magnetic state of the overall exchange-coupled system and not just the individual lanthanide ions consistent with a giant-spin interpretation of the magnetic state.

Conclusions

In summary, the use of the $tz^{\bullet-}$ as a bridging ligand of $[Cp^*_2Dy^{III}]^+$ moieties led to the isolation of a new family of radical bridged dinuclear metallocenes. This family of complexes is only the second example of the radical form of the 1,2,4,5-tetrazine in the literature. Strong antiferromagnetic coupling between the Ln^{III} ions, mediated by the diffuse π^* orbitals of the tetrazinyl ring, yielded a strong $J_{Gd\text{-}rad}$ of -7.22 cm^{-1} in **1**, which is even comparable to some dinitrogen-bridged complexes with similar exchange strengths (-7.2 and -7.3 cm^{-1}).[14] For **2** and **3**, ac magnetic susceptibility measurements revealed that these SMMs relax slowly *via* thermally activated processes, through the first excited KDs. Using computational studies, it was found that these KDs correspond to an Ising-type ferrimagnetic spin configuration where the magnetic moments of the Ln^{III} ions are co-aligned while the magnetic moment of the radical pointing to the opposite direction, supporting the proposed *J* model. As such, **2** and **3** relax as a magnetic entity rather than weakly coupled individual spins. The U_{eff} that were obtained for **2** and **3** are higher compared to other tetrazine-based radical bridged Ln systems proving that the unexplored unsubstituted $tz^{\bullet-}$ ligand can provide new aspects in molecular magnetism towards the synthesis of new high performing SMMs.

Conflicts of interest

There are no conflicts to declare.

Acknowledgements

The authors thank the University of Ottawa, the Canada Foundation for Innovation (CFI) and Natural Sciences and Engineering Research Council of Canada (NSERC) for the financial support of this work. N. M. acknowledges the University of Ottawa and the Stavros Niarchos Foundation for financial support through scholarships. A. M. acknowledges funding provided by the Academy of Finland (grant no. 332294) and the University of Oulu (Kvantum Institute). Computational resources were provided by CSC-IT Center for Science in Finland and the Finnish Grid and Cloud Infrastructure (persistent identifier urn:nbn:fi:research-infras-2016072533).

References

1 E. Coronado, Molecular magnetism: from chemical design to spin control in molecules, materials and devices, *Nat. Rev. Mater.*, 2020, **5**, 87–104.
2 N. F. Chilton, Molecular Magnetism, *Annu. Rev. Mater. Res.*, 2022, **52**, 79–101.
3 K. L. M. Harriman, D. Errulat and M. Murugesu, Magnetic Axiality: Design Principles from Molecules to Materials, *Trends Chem.*, 2019, **1**, 425–439.
4 C. J. Milios, A. Vinslava, W. Wernsdorfer, S. Moggach, S. Parsons, S. P. Perlepes, G. Christou and E. K. Brechin, A Record Anisotropy Barrier for a Single-Molecule Magnet, *J. Am. Chem. Soc.*, 2007, **129**, 2754–2755.
5 P. Kumar, S. Biswas, A. Swain, J. Acharya, V. Kumar, P. Kalita, J. F. Gonzalez, O. Cador, F. Pointillart, G. Rajaraman and V. Chandrasekhar, Azide-Coordination in Homometallic Dinuclear Lanthanide(III) Complexes Containing Nonequivalent Lanthanide Metal Ions: Zero-Field SMM Behavior in the Dysprosium Analogue, *Inorg. Chem.*, 2021, **60**, 8530–8545.
6 G. Cucinotta, M. Perfetti, J. Luzon, M. Etienne, P.-E. Car, A. Caneschi, G. Calvez, K. Bernot and R. Sessoli, Magnetic Anisotropy in a Dysprosium/DOTA Single-Molecule Magnet: Beyond Simple Magneto-Structural Correlations, *Angew. Chem. Int. Ed.*, 2012, **51**, 1606–1610.
7 C. A. P. Goodwin, F. Ortu, D. Reta, N. F. Chilton and D. P. Mills, Molecular magnetic hysteresis at 60 kelvin in dysprosocenium, *Nature*, 2017, **548**, 439–442.
8 F.-S. Guo, B. M. Day, Y.-C. Chen, M.-L. Tong, A. Mansikkamäki and R. A. Layfield, A Dysprosium Metallocene Single-Molecule Magnet Functioning at the Axial Limit, *Angew. Chem. Int. Ed.*, 2017, 5.
9 J. Liu, Y.-C. Chen, J.-L. Liu, V. Vieru, L. Ungur, J.-H. Jia, L. F. Chibotaru, Y. Lan, W. Wernsdorfer, S. Gao, X.-M. Chen and M.-L. Tong, A Stable Pentagonal Bipyramidal Dy(III) Single-Ion Magnet with a Record Magnetization Reversal Barrier over 1000 K, *J. Am. Chem. Soc.*, 2016, **138**, 5441–5450.
10 F.-S. Guo, B. M. Day, Y.-C. Chen, M.-L. Tong, A. Mansikkamäki and R. A. Layfield, Magnetic hysteresis up to 80 kelvin in a dysprosium metallocene single-molecule magnet, *Science*, 2018, **362**, 1400–1403.
11 A. B. Canaj, S. Dey, E. R. Martí, C. Wilson, G. Rajaraman and M. Murrie, Insight into D6h Symmetry: Targeting Strong Axiality in Stable Dysprosium(III) Hexagonal Bipyramidal Single-Ion Magnets, *Angew. Chem. Int. Ed.*, 2019, **58**, 14146–14151.
12 S. K. Gupta, T. Rajeshkumar, G. Rajaraman and R. Murugavel, An air-stable Dy(III) single-ion magnet with high anisotropy barrier and blocking temperature, *Chem. Sci.*, 2016, **7**, 5181–5191.
13 C. A. Gould, K. R. McClain, D. Reta, J. G. C. Kragskow, D. A. Marchiori, E. Lachman, E.-S. Choi, J. G. Analytis, R. D. Britt, N. F. Chilton, B. G. Harvey and J. R. Long, Ultrahard magnetism from mixed-valence dilanthanide complexes with metal-metal bonding, *Science*, 2022, **375**, 198–202.
14 S. Demir, M. I. Gonzalez, L. E. Darago, W. J. Evans and J. R. Long, Giant coercivity and high magnetic blocking temperatures for N 2 3− radical-bridged dilanthanide complexes upon ligand dissociation, *Nat. Commun.*, 2017, **8**, 2144.
15 B. S. Dolinar, D. I. Alexandropoulos, K. R. Vignesh, T. James and K. R. Dunbar, Lanthanide Triangles Supported by Radical Bridging Ligands, *J. Am. Chem. Soc.*, 2018, **140**, 908–911.
16 B. S. Dolinar, S. Gómez-Coca, D. I. Alexandropoulos and K. R. Dunbar, An air stable radical-bridged dysprosium single molecule magnet and its neutral counterpart: redox switching of magnetic relaxation dynamics, *Chem. Commun.*, 2017, **53**, 2283–2286.

17 P. Zhang, M. Perfetti, M. Kern, P. P. Hallmen, L. Ungur, S. Lenz, M. R. Ringenberg, W. Frey, H. Stoll, G. Rauhut and J. van Slageren, Exchange coupling and single molecule magnetism in redox-active tetraoxolene-bridged dilanthanide complexes, *Chem. Sci.*, 2018, **9**, 1221–1230.

18 C. A. Gould, E. Mu, V. Vieru, L. E. Darago, K. Chakarawet, M. I. Gonzalez, S. Demir and J. R. Long, Substituent Effects on Exchange Coupling and Magnetic Relaxation in 2,2'-Bipyrimidine Radical-Bridged Dilanthanide Complexes, *J. Am. Chem. Soc.*, 2020, **142**, 21197–21209.

19 J. D. Rinehart, M. Fang, W. J. Evans and J. R. Long, Strong exchange and magnetic blocking in N23−-radical-bridged lanthanide complexes, *Nat. Chem.*, 2011, **3**, 538–542.

20 N. Mavragani, D. Errulat, D. A. Gálico, A. A. Kitos, A. Mansikkamäki and M. Murugesu, Radical-Bridged Ln4 Metallocene Complexes with Strong Magnetic Coupling and a Large Coercive Field, *Angew. Chem. Int. Ed.*, 2021, **60**, 24206–24213.

21 O. Stetsiuk, A. Abhervé and N. Avarvari, 1,2,4,5-Tetrazine based ligands and complexes, *Dalton Trans.*, 2020, **49**, 5759–5777.

22 N. Mavragani, A. A. Kitos, J. L. Brusso and M. Murugesu, Enhancing Magnetic Communication between Metal Centres: The Role of s-Tetrazine Based Radicals as Ligands, *Chem. Eur. J.*, 2021, **27**, 5091–5106.

23 C. A. Gould, L. E. Darago, M. I. Gonzalez, S. Demir and J. R. Long, A Trinuclear Radical-Bridged Lanthanide Single-Molecule Magnet, *Angew. Chem. Int. Ed.*, 2017, **56**, 10103–10107.

24 S. Demir, M. Nippe, M. I. Gonzalez and J. R. Long, Exchange coupling and magnetic blocking in dilanthanide complexes bridged by the multi-electron redox-active ligand 2,3,5,6-tetra(2-pyridyl)pyrazine, *Chem. Sci.*, 2014, **5**, 4701–4711.

25 S. Demir, J. M. Zadrozny, M. Nippe and J. R. Long, Exchange Coupling and Magnetic Blocking in Bipyrimidyl Radical-Bridged Dilanthanide Complexes, *J. Am. Chem. Soc.*, 2012, **134**, 18546–18549.

26 F. Bertinotti, C. Giacomello and A. M. Liquori, The structure of heterocyclic compounds containing nitrogen. I. Crystal and molecular structure of s-tetrazine, *Acta Cryst.*, 1956, **9**, 510–514.

27 G. Brunet, M. Hamwi, M. A. Lemes, B. Gabidullin and M. Murugesu, A tunable lanthanide cubane platform incorporating air-stable radical ligands for enhanced magnetic communication, *Commun. Chem.*, 2018, **1**, 1–6.

28 J. J. McKinnon, A. S. Mitchell and M. A. Spackman, Hirshfeld Surfaces: A New Tool for Visualising and Exploring Molecular Crystals, *Chem. Eur. J.*, 1998, **4**, 2136–2141.

29 N. F. Chilton, R. P. Anderson, L. D. Turner, A. Soncini and K. S. Murray, PHI: A powerful new program for the analysis of anisotropic monomeric and exchange-coupled polynuclear d- and f-block complexes, *J. Comput. Chem.*, 2013, **34**, 1164–1175.

30 D. Reta and N. F. Chilton, Uncertainty estimates for magnetic relaxation times and magnetic relaxation parameters, *Phys. Chem. Chem. Phys.*, 2019, **21**, 23567–23575.

31 L. Noodleman, Valence bond description of antiferromagnetic coupling in transition metal dimers, *J. Chem. Phys.*, 1981, **74**, 5737–5743.

32 G. Jonkers, C. A. de Lange, L. Noodleman and E. J. Baerends, Broken symmetry effects in the He(I) valence photoelectron spectrum of Se(CN)2, *Mol. Phys.*, 1982, **46**, 609–620.

33 L. Noodleman, J. G. Norman, J. H. Osborne, A. Aizman and D. A. Case, Models for ferredoxins: electronic structures of iron-sulfur clusters with one, two, and four iron atoms, *J. Am. Chem. Soc.*, 1985, **107**, 3418–3426.

34 L. Noodleman and E. R. Davidson, Ligand spin polarization and antiferromagnetic coupling in transition metal dimers, *Chem. Phys.*, 1986, **109**, 131–143.

35 I. de P. R. Moreira and F. Illas, A unified view of the theoretical description of magnetic coupling in molecular chemistry and solid state physics, *Phys. Chem. Chem. Phys.*, 2006, **8**, 1645–1659.

36 H. Xiang, C. Lee, H.-J. Koo, X. Gong and M.-H. Whangbo, Magnetic properties and energy-mapping analysis, *Dalton Trans.*, 2013, **42**, 823–853.

37 T. Yanai, D. P. Tew and N. C. Handy, A new hybrid exchange–correlation functional using the Coulomb-attenuating method (CAM-B3LYP), *Chem. Phys. Lett.*, 2004, **393**, 51–57.

38 A. D. Becke, Density-functional exchange-energy approximation with correct asymptotic behavior, *Phys. Rev. A*, 1988, **38**, 3098–3100.

39 C. Lee, W. Yang and R. G. Parr, Development of the Colle-Salvetti correlation-energy formula into a functional of the electron density, *Phys. Rev. B*, 1988, **37**, 785–789.

40 F. Neese, Software update: the ORCA program system, version 4.0, *WIREs Comput. Mol. Sci.*, 2018, **8**, e1327.

41 F. Neese, F. Wennmohs, U. Becker and C. Riplinger, The ORCA quantum chemistry program package, *J. Chem. Phys.*, 2020, **152**, 224108.

42 F. Neese, The SHARK integral generation and digestion system, *J. Comput. Chem.*, 2022, **1**, in press, DOI:10.1002/jcc.26942.

43 a) B. O. Roos in *Advances in Chemical Physics*, *Ab Initio Methods in Quantum Chemistry II*, Vol. 69 (Ed.: K. P. Lawley), Wiley, New York, 1987, pp. 399–455; b) P. Siegbahn, A. Heiberg, B. Roos and B. Levy, A Comparison of the Super-CI and the Newton-Raphson Scheme in the Complete Active Space SCF Method, *Phys. Scr.*, 1980, **21**, 323–327.

44 B. O. Roos, P. R. Taylor and P. E. M. Sigbahn, A complete active space SCF method (CASSCF) using a density matrix formulated super-CI approach, *Chem. Phys.*, 1980, **48**, 157–173.

45 a) P. E. M. Siegbahn, J. Almlöf, A. Heiberg and B. O. Roos, The complete active space SCF (CASSCF) method in a Newton–Raphson formulation with application to the HNO molecule, *J. Chem. Phys.*, 1981, **74**, 2384–2396; b) B. O. Roos, R. Lindh, P. Å. Malmqvist, V. Veryazov and P.-O. Widmark, *Multiconfigurational Quantum Chemistry,* Wiley, Hoboken, NJ, **2016**.

46 C. Angeli, R. Cimiraglia, S. Evangelisti, T. Leininger and J.-P. Malrieu, Introduction of n-electron valence states for multireference perturbation theory, *J. Chem. Phys.*, 2001, **114**, 10252–10264.

47 C. Angeli, R. Cimiraglia and J.-P. Malrieu, N-electron valence state perturbation theory: a fast implementation of the strongly contracted variant, *Chem. Phys. Lett.*, 2001, **350**, 297–305.

48 C. Angeli, R. Cimiraglia and J.-P. Malrieu, n-electron valence state perturbation theory: A spinless formulation and an efficient implementation of the strongly contracted and of the partially contracted variants, *J. Chem. Phys.*, 2002, **117**, 9138–9153.

49 F. Neese, T. Petrenko, D. Ganyushin and G. Olbrich, Advanced aspects of ab initio theoretical optical spectroscopy of transition metal complexes: Multiplets, spin-orbit coupling and resonance Raman intensities, *Coord. Chem. Rev.*, 2007, **251**, 288–327.

50 M. Atanasov, D. Aravena, E. Suturina, E. Bill, D. Maganas and F. Neese, First principles approach to the electronic structure, magnetic anisotropy and spin relaxation in mononuclear 3d-transition metal single molecule magnets, *Coord. Chem. Rev.*, 2015, **289–290**, 177–214.

51 a) N. Iwahara and L. F. Chibotaru, Exchange interaction between J multiplets, *Phys. Rev. B*, 2015, **91**, 174438; b) L. F. Chibotaru

in S. A. Rice, A. R. Dinner (Eds.) *Advances in Chemical Physics, Volume 153*, Wiley, 2013, pp. 397–519.

52 a) M. E. Lines, Orbital Angular Momentum in the Theory of Paramagnetic Clusters, *J. Chem. Phys.*, 1971, **55**, 2977–2984; b) L. Ungur and L. F. Chibotaru, Computational *Modelling of Magnetic Properties of Lanthanide Compounds* in *Lanthanide and Actinides in Molecular Magnetism.* Eds. R. A. Layfield and M. Murugesu, Wiley,-VHC, Weinheim, Germany, 2015.

53 V. Vieru, N. Iwahara, L. Ungur and L. F. Chibotaru, Giant exchange interaction in mixed lanthanides, *Sci. Rep.*, 2016, **6**, 24046.

54 G. T. Nguyen and L. Ungur, Understanding the magnetization blocking mechanism in N_2^{3-} -radical-bridged dilanthanide single-molecule magnets, *Phys. Chem. Chem. Phys.*, 2021, **23**, 10303–10310.

55 G. T. Nguyen and L. Ungur, The Role of Radical Bridges in Polynuclear Single-Molecule Magnets, *Chem. Eur. J.*, 2022, **28**, e202200227.

56 L. Ungur, M. Thewissen, J.-P. Costes, W. Wernsdorfer and L. F. Chibotaru, Interplay of Strongly Anisotropic Metal Ions in Magnetic Blocking of Complexes, *Inorg. Chem.*, 2013, **52**, 6328–6337.

